*applied sciences*

MDPI

*Article*

# Crustal Thinning Characteristics Beneath the Weihe Graben

**Longyun Chen [1,2], Shuwen Dong [1,*], Yaocen Pan [1,*] and Wei Shi [1]**

[1] State Key Laboratory of Deep Earth and Mineral Exploration, Chinese Academy of Geological Sciences, Beijing 100037, China; 3020230001@email.cugb.edu.cn (L.C.); shiweinmg@163.com (W.S.)
[2] School of Earth Sciences and Resources, China University of Geosciences (Beijing), Beijing 100083, China
* Correspondence: swdong8888@126.com (S.D.); panyaocen@hotmail.com (Y.P.)

**Abstract**

The Weihe Graben lies on the northern margin of the Qinling Orogenic Belt, the collisional suture between the North China Craton and South China Block, and records Cenozoic extensional overprinting of its earlier tectonic evolution. We integrate deep seismic reflection profiles and tomographic datasets to characterize heterogeneous lithospheric modification and elucidate the geodynamics of post-orogenic crustal thinning and graben formation. A single Moho occurs beneath the Dabashan and southern Ordos Block, where crustal thickness exceeds 43 km, whereas a distinctive double-Moho structure occurs beneath the Weihe Graben. Its upper and lower interfaces reach depths of 36 and 51 km, respectively, defining a ~15 km–thick lenticular transitional layer. Low–velocity and low–resistivity anomalies in the upper mantle indicate Cenozoic asthenospheric upwelling beneath the region. Our results suggest that mantle upwelling promoted regional crustal thinning, while the Moho doublet mainly reflects eclogite relics and subsequent modification. Since the Eocene, the stress regime changed from compression to extension, associated with far–field Pacific Plate subduction and continuous counter-clockwise rotation of the Ordos Block. Block rotation promoted lithospheric tearing along its southeastern margin and destabilization of the crust–mantle boundary, facilitating mantle upwelling. Pre–existing Late Triassic–Middle Jurassic thrust faults were selectively reactivated, with northern boundary faults transformed into listric normal faults, ultimately forming the extensional Weihe Graben and accompanying differential uplift of the northern Qinling Block and graben margins.

**Keywords:** Weihe Graben; deep seismic reflection; Moho doublet; crustal thinning; eclogitic lower-crustal remnants; lithospheric evolution

## 1. Introduction

The Weihe Graben, located in central China between the southern Ordos Block and the Qinling Orogenic Belt, forms a major tectonic component of the southern Fenwei Rift System. Situated near the tectonic transition between the North China Craton and the South China Block, it records the superposition of the long-term evolution of the Qinling orogenic belt and subsequent Cenozoic extensional deformation [1–5]. Over the past several decades, the Weihe Graben and its adjacent areas have been extensively studied, and multiple models have been proposed to explain its tectonic evolution. Nevertheless, considerable debate remains over the mechanisms responsible for its formation [6–9]. Its unique tectonic setting makes the region an ideal natural laboratory for investigating intracontinental deformation, plate-boundary interactions, and crust–mantle dynamics in the Chinese mainland [10]. Since the Mesozoic, this region has undergone a fundamental transition from a compressional crust-thickening regime to an extensional crust-thinning regime, recording

Check for updates

Academic Editor: Andrea Di Capua

Received: 14 August 2026
Revised: 14 September 2026
Accepted: 18 September 2026
Published: 21 September 2026

**Copyright:** © 2026 by the authors. Licensee MDPI, Basel, Switzerland. This article is an open access article distributed under the terms and conditions of the Creative Commons Attribution (CC BY) license.

a complex and representative tectonic evolutionary history [11,12]. During the Cenozoic, influenced by the far-field effects of the India–Eurasia collision and the westward rollback of the Pacific Plate, the Weihe Graben evolved into a typical intracontinental fault-bounded basin. Its tectonic evolution is closely linked to deep crust–mantle processes [13–15].

Deep seismic exploration provides a key approach to resolving crust–upper mantle architecture and constraining the geodynamic mechanisms of intracontinental basins, and provides critical constraints on the deep crust–mantle structure and tectonic evolution of the Weihe Graben [10,16,17]. Previous wide-angle reflection/refraction seismic profiles have revealed pronounced Moho uplift beneath the Weihe Graben, with crustal thickness locally reduced to approximately 32 km [18–20]. Compared with the relatively stable Ordos Block (~43 km crustal thickness) [21,22] and the tectonically thickened Dabashan Orogenic Belt (~45 km crustal thickness) [23,24], the Weihe Graben is characterized by pronounced crustal thinning and strong lateral variations in crustal thickness. Subsequent receiver-function studies have further supported the overall pattern of crustal thinning in the study area [20]. Meanwhile, typical geophysical signatures of intracrustal low-velocity anomalies and upper-mantle high-velocity material intrusion have been detected in the deep graben, offering direct observational evidence for regional mantle activity [7].

Existing geophysical observations generally interpret such anomalous structures as a geophysical manifestation of deep mantle upwelling, suggesting that the development of the Weihe Graben was accompanied by intense crust–mantle material exchange and dynamic interaction [12]. Nevertheless, several key issues remain unresolved: it is still poorly understood how mantle upwelling modulates Moho undulation and couples deep geodynamic processes with crustal extension and thinning, and no consensus has yet been reached regarding the fine-scale architecture, physical properties, and evolutionary mechanism of the Moho discontinuity. The lack of critical deep constraints on these underlying geodynamic processes continues to hinder a comprehensive understanding of the Cenozoic deep geodynamic evolution of the Weihe Graben [25].

Based on newly acquired high-resolution deep seismic reflection profile data, this study identifies a well-defined Moho doublet beneath the Weihe Graben. This distinctive deep feature is characterized by two clearly distinguishable sets of lenticular, high-amplitude seismic reflectors. We systematically characterize the spatial distribution, geometric morphology, and seismic response characteristics of the Moho doublet within the Weihe Graben. By integrating multidimensional geophysical constraints, including regional shear-wave velocity ($V_S$), compressional-wave velocity ($V_P$), and resistivity, we further investigate the potential coupling between the Moho doublet and deep crust–mantle processes, and assess the deep geodynamic processes responsible for its formation. This work provides new, high-resolution observational constraints for re-evaluating the Cenozoic crust–mantle evolution, the development of the intracontinental fault-bounded Weihe Graben, and regional tectonic dynamics. The results also have broader implications for understanding the geodynamic evolution of the Fenwei Rift System and intracontinental extensional tectonics in eastern China. The key novelty of this study lies in the discovery of a well-defined Moho doublet beneath the Weihe Graben based on newly acquired high-resolution deep seismic reflection data, providing direct geophysical evidence for crust–mantle material exchange and dynamic coupling, and offering a new perspective on the deep geodynamic evolution of intracontinental extensional basins.

## 2. Geological Setting

The north–south seismic profile in this study originates in northern Sichuan, extends northward across the Daba Shan Orogenic Belt, the Qinling Orogenic Belt, and the Weihe Graben, and terminates along the southern margin of the Ordos Block [26] (Figure 1). The

basements of the Qinling Orogen and the Weihe Graben have undergone multiple phases of Paleozoic tectonic overprinting. This region represents a key tectonic zone formed through the amalgamation of the North China Plate and the South China Plate, during which the regional tectonic basement was established [2,27]. The tectonic units surrounding the study area also underwent broadly synchronous evolution. To the south, the Dabashan Tectonic Belt constitutes the frontal transitional zone along the northern margin of the South China Plate [24], with its folded basement developing in association with the Paleozoic evolution of the Qinling Ocean basin. To the north, the Ordos Block has long maintained stable cratonic characteristics and constitutes the stable basement unit in the northern part of the study region, exhibiting a pronounced tectonic contrast with the Qinling Orogenic Belt and the Weihe transitional zone [28].

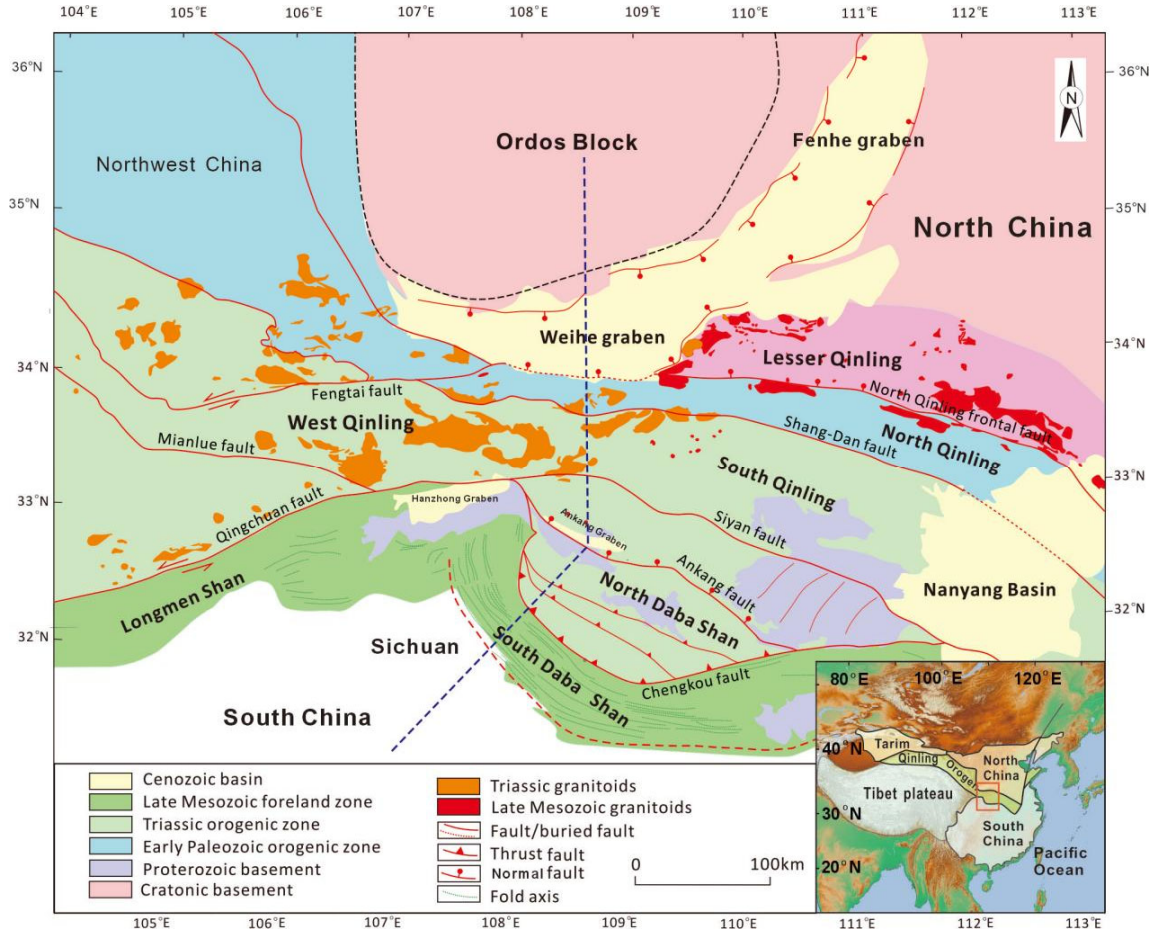



**Figure 1.** Simplified geologic map of the Qinling Orogenic Belt, Central China. The blue dotted line marks the trace of the reflection seismic profile illustrated in Figure 2.

An ancient crystalline basement was established across the region during the Archean–Paleoproterozoic. Influenced by the evolution of the Tethyan Ocean, rift systems and continental-margin sedimentary sequences developed within the Qinling Orogen from the Mesoproterozoic to the Late Paleozoic [2,29]. At the end of the Triassic, the Mianlue Ocean basin was completely closed, marking the final collisional amalgamation of the North China Plate and the South China Plate and the termination of the main orogenic stage of the Qinling Orogen. This event marked a fundamental transition from ocean–continent tectonics to an intracontinental orogenic regime [6]. During the Yanshanian orogeny (Jurassic–Cretaceous), the Qinling Orogenic Belt experienced intense intracontinental compression, folding, uplift, and magmatic emplacement. Large-scale fault systems

and granitic plutons developed, and the mountain range acquired its primary topographic character [26,30]. Under regional plate compression, the Dabashan area underwent intense fold-and-thrust deformation, forming a foreland fold-and-thrust belt. The Ordos Block experienced overall stable uplift, with tectonic reworking largely confined to its margins [31]. During the same period, under north–south compressional deformation, the basement strata in the Weihe area experienced intense folding and faulting. Only small-scale fault-controlled depocenters developed locally during the Mesozoic, and no large-scale basin had yet formed; instead, the region was dominated by basement uplift and erosional modification [32].

Since the Cenozoic, the regional tectonic regime has shifted from Mesozoic compressional tectonics to Cenozoic extension and faulting. Driven by the far-field effects of Tibetan Plateau uplift and Pacific Plate subduction, the Qinling orogen and the Weihe Graben subsequently underwent differential tectonic evolution [33]. Since the Paleogene, a predominantly east–west extensional stress regime has prevailed across the region. Pre-existing Yanshanian fault systems were reactivated, and a series of extensional normal faults, including the North Qinling Piedmont Fault and the Weihe Fault, became intensely active, promoting pronounced north–south tectonic differentiation [27]. The Qinling Orogenic Belt underwent persistent episodic rapid uplift accompanied by intense weathering and erosion, gradually developing its present-day high-relief mountainous topography, while only scattered continental sediments were preserved in local intermontane depressions [34]. In contrast, the Weihe area north of these faults underwent intense fault-controlled subsidence, leading to the development of the Cenozoic Weihe Graben. The graben exhibits a typical half-graben geometry, with a fault-controlled southern margin and an onlapping northern margin, while its depocenter migrated progressively in response to ongoing tectonic activity. From the Neogene to the Quaternary, tectonic activity further intensified. Episodic uplift of the Qinling Orogen persisted, driving continuous erosion and northward transport of detrital material into the Weihe Graben, where rapid subsidence resulted in the accumulation of exceptionally thick sedimentary successions [35].

## 3. Data and Methods

### *3.1. Data Acquisition*

Field seismic observations were performed using the Sercel SN408XL 24-bit digital seismic acquisition system (Sercel, Carquefou, France) with a total of 1600 observation channels. Differentiated source layouts were adopted for basin and mountain landforms, including conventional 40 kg explosive charges and 200 kg large–yield combined charges. The core acquisition parameters are summarized in Table 1. Uniformly, 10 Hz SM-24 geophones were deployed at a 40 m trace interval with a 12–element linear array over an 11 m span to suppress surface waves. The instrument was set to a fixed sampling interval of 2 ms and a recording duration of 30 s, with a 15 Hz low–cut filter and a 250 Hz high–cut filter enabled, while the notch filter was disabled.

**Table 1.** Summary of Core Seismic Acquisition Parameters.

| Category | Key Settings |
|---|---|
| Instrument | Sercel SN408XL, 24-bit, 1600 channels |
| Source | 40 kg conventional charges; 200 kg large charges |
| Shot Depth | 22–24 m (40 kg); 25 m (200 kg) |
| Fold | 60-fold (basin); 120-fold (mountain) |
| Geophones | 10 Hz SM-24; 40 m spacing; 12–element array |
| Recording | 2 ms sampling; 30 s record length |
| Filters | 15 Hz low–cut; 250 Hz high–cut; notch off |

### *3.2. Data Processing*

#### 3.2.1. Seismic Processing

Seismic data were processed using Grisys, Omega, and CGG following a standard workflow, including geometry definition, trace editing, amplitude compensation, static correction, filtering, velocity analysis, NMO correction, residual static correction, stacking, and pre-stack migration.

Spherical divergence compensation and interactive muting were applied for amplitude balancing and noise suppression. Elevation static correction used a replacement velocity of 4000 m/s and a datum elevation of 1200 m. An 8–12–65–70 Hz band-pass filter was applied to shallow reflections. Residual static correction was performed using the STACK–POWER iterative algorithm. The final seismic profiles were plotted at 6 km/s without vertical exaggeration.

#### 3.2.2. Mountain Correction and Migration

For mountainous areas, the TSCWR finite-difference static correction method was applied to reduce topography-related distortions and imaging shadows. A modified Kirchhoff pre-stack time migration (KPSTM) algorithm was subsequently used to improve imaging under complex terrain and low-SNR conditions, effectively suppressing terrain-related migration artifacts and enhancing the continuity of deep reflections.

## 4. Seismic Characteristics and Findings

We acquired a complete north–south deep seismic reflection profile (Figure 2), approximately 485 km long, through the SINOPROBE Project (shown by the blue dashed line in Figure 1). This profile originates in the northern Sichuan Basin, runs northward across the Dabashan Orogenic Belt, the North Qinling Orogenic Belt and the Weihe Graben, and terminates at the southern margin of the Ordos Block. Segments of this profile overlap with previously published seismic lines [20,23,24,26]. Integrated with travel-time tomographic data from large-charge wide-angle seismic experiments, this paper systematically characterizes the spatial distribution of reflective wave groups from the upper-middle crust, lower crust and crust–mantle boundary (Moho discontinuity) for segmented tectonic domains across the study area.

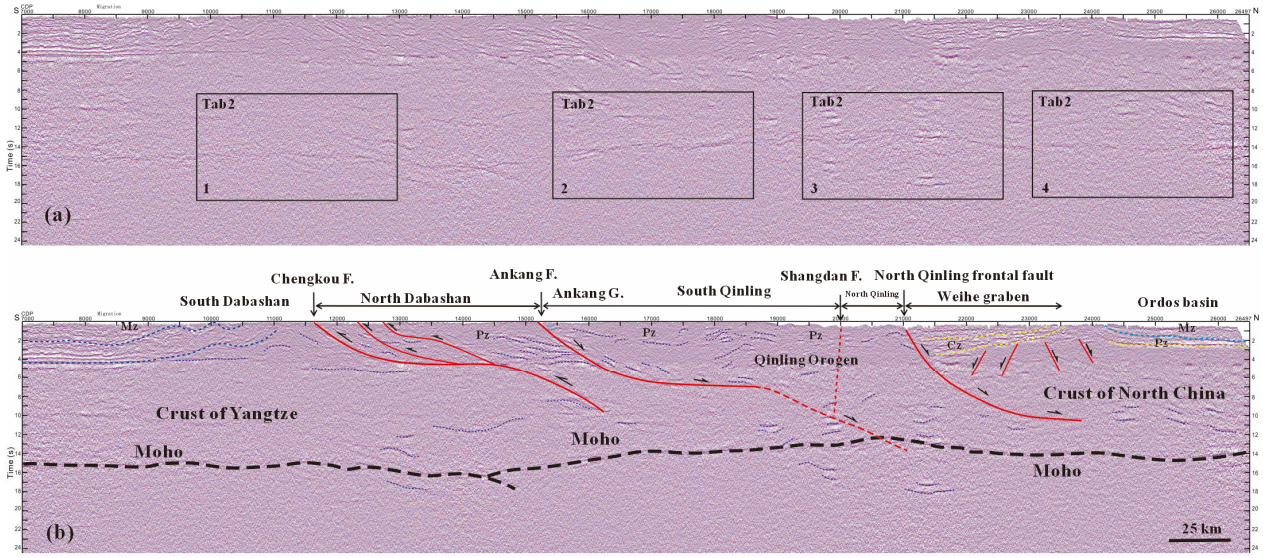



**Figure 2.** Uninterpreted (**a**) and interpreted (**b**) migrated seismic reflection profile across the entire Qinling Orogen. This profile integrates the southern section of Dong et al. (2013) and Li et al. (2015), and the northern section of Li et al. (2017) and Zhang et al. (2022) [20,23,24,26].

Seismic observations reveal prominent regional variations in intracrustal reflection signatures and velocity fields among different tectonic units. A distinctive Moho doublet is imaged beneath the North Qinling Orogenic Belt and the Weihe Graben segments, whereas both the South China Block and the Ordos Craton exhibit a single, continuous Moho discontinuity.

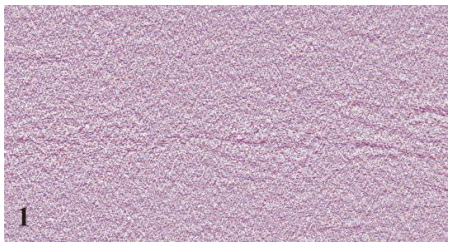
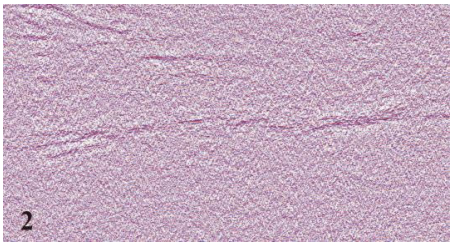
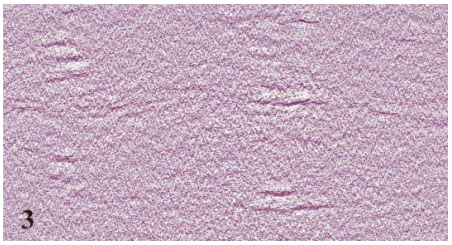
### *4.1. Seismic Reflection Imaging Characteristics*

#### 4.1.1. Features of the Crust–Mantle Boundary

Moho reflective phases can be continuously traced along the entire profile. The Moho discontinuities of different tectonic units show marked differences in layer number, two-way travel time (TWT), continuity and undulation, and the Moho features of each segment are summarized in Table 2. The segmented characteristics are described as follows:

(1) Sichuan Basin–Dabashan Orogenic Belt

**Table 2.** Moho Structural Characteristics of Different Tectonic Units.

| Tectonic Unit | Moho Characteristics | Key Data Example |
| --- | --- | --- |
| Sichuan Basin—Dabashan Orogen | Single continuous Moho at 45 km depth, with a thin, laterally uniform crust–mantle transition zone. |   |
| South Qinling | Moho shallows northward from 45 to 40 km, with undulating geometry and local fault offsets; the crust thickens southward. |   |
| North Qinling-Weihe Graben | Moho doublet (~36 km shallow Moho; ~51 km lower reflector); Moho follows basement relief and is disrupted by lithosphere-scale faults. |   |
| Southern Ordos Block | Single, flat and continuous Moho at 42~44 km depth, with no obvious offsets, indicating a stable crust–mantle boundary. |   |

In the Sichuan Basin–Dabashan Orogenic Belt, receiver-function imaging reveals a Moho at a depth of approximately 45 km, characterized by a relatively flat and continuous geometry. The crust–mantle transition is relatively narrow and laterally homoge-

neous, without distinct secondary conversion interfaces. A localized disruption of the Moho is observed south of the Ankang Basin, indicating spatial heterogeneity in the deep crustal structure.

(2) South Qinling Orogenic Belt

Beneath the southern South Qinling adjacent to the South China Block, corresponding to the Sichuan Basin–Dabashan orogenic belt segment, the Moho is located at a depth of approximately 45 km and is characterized by a relatively flat and laterally continuous crust–mantle boundary. The crust–mantle transition zone is relatively thin and laterally homogeneous, without obvious secondary interfaces. Further northward into the interior of South Qinling, the Moho progressively shallows and the crust gradually thins. The crust–mantle boundary becomes increasingly undulatory and is characterized by a more pronounced crust–mantle transition zone. The Moho reaches its shallowest depth of ~38 km in the northern South Qinling, immediately south of the Shangdan Suture Zone, where the crust is correspondingly thinnest. Overall, the crustal structure beneath South Qinling exhibits a pronounced south-to-north variation, characterized by a relatively thick crust with a simple and laterally continuous Moho in the south, transitioning northward into a thinner crust with a more undulatory crust–mantle boundary and a well-developed crust–mantle transition zone. Local disturbances of the Moho may also be associated with deep faulting.

(3) North Qinling Orogenic Belt-Weihe Graben

Crustal thickness decreases northward across the Qinling Orogenic Belt [36]. North of the Shangdan Fault, the single Moho reflection becomes indistinct and is replaced by two sets of lenticular, high-amplitude reflective interfaces, which together define a typical Moho doublet. The shallow Moho has two-way travel times of 12.4~13.0 s, corresponding to depths of approximately 36~38 km, whereas the lower reflector has two-way travel times of 17–18 s, corresponding to depths of approximately 49~52 km. The depth interval between the two interfaces corresponds to a ~15 km-thick, densely reflective crust–mantle transition zone. The shallow Moho exhibits good lateral continuity, whereas the lower reflector is less continuous and exhibits only gentle, fold-like undulations beneath the Shangdan Suture Zone.

The Moho doublet of North Qinling extends into the Weihe Graben, and the two reflective interfaces exhibit broadly synchronous undulations that follow the relief of the graben basement. Beneath the depocenter of the Xi'an sedimentary sag, both reflective interfaces are broadly uplifted, while the vertical separation between them increases. In the Li Shan and Bei Shan uplifted areas on both sides of the graben, both Moho reflectors deepen, while the thickness of the intervening transition zone increases. Several steeply dipping major deep faults cut through the Moho doublet beneath the Weihe Graben. Seismic reflection amplitudes decay markedly on both sides of the fault zones, and numerous inclined, sheet-like reflectors are developed within the fault zones [18].

(4) Southern Ordos Block

The double high-amplitude reflective structure disappears within the Ordos Block, where it is replaced by a single, relatively flat Moho discontinuity. Two-way travel times range from 13.8 to 14.4 s, corresponding to crustal thicknesses of approximately 42~44 km. The Moho is generally flat, with little evidence of fault-related offset. Reflective signals within the crust–mantle transition zone are weak, and no superimposed crust–mantle reflections are observed, reflecting the stable and rigid crust–mantle boundary characteristic of an ancient craton.

Previous deep seismic reflection profiling across the Daba Shan thrust belt revealed pronounced lateral variations in Moho geometry. The Moho exhibits wavy undulations

beneath the southern part of the profile adjacent to the Sichuan Basin, whereas distinct vertical offsets occur beneath the northern thrust belt, where deep thrust shear zones penetrate the crust–mantle boundary [23]. These Moho-offsetting structures show no direct structural linkage with upper-crustal thrusts and folds. In addition, seismically transparent bodies interpreted as eclogitized mafic intrusions are distributed within the lower crust immediately above the Moho discontinuity.

This deep anomalous body beneath the graben exhibits a lenticular shape with limited lateral extent and tapered terminations, indicating that it does not represent a conventional continuous crust−mantle transition zone but instead corresponds to a residual deep tectonic unit with distinct physical properties.

#### 4.1.2. Reflection Characteristics of the Upper-Middle Crust

In this study, the depth above 20 km is defined as the upper–middle crust, and that below 20 km is defined as the lower crust. Seismic reflections within the upper–middle crust of the study area are mainly derived from sedimentary sequences, thrust–nappe structures, and extensional fault-blocks, with distinct segmented reflection features preserved across different tectonic domains (Figure 3). The upper crust of the Sichuan Basin is dominated by continuous, sub–horizontal reflections originating from sedimentary strata, and the maximum sedimentary thickness of the Ankang Graben reaches 3 km [37]. South of the Ankang Graben, south-dipping imbricate thrust reflection structures are recognized, corresponding to the thin-skinned foreland nappe system of the Dabashan Orogenic Belt. The North Qinling Orogenic Belt constitutes an integrated fault–block mountain range with relatively homogeneous internal structures, which are mainly composed of Precambrian metamorphic basement and Paleozoic granitoids [2]. The upper crust of the Weihe Graben is dissected by multiple listric normal faults, producing an alternating pattern of small-scale grabens and horsts. Distinct layered reflections from Cenozoic strata are observed, with a maximum sedimentary thickness of approximately 7 km. In the southern Ordos Block, the crystalline basement yields flat and continuous reflections, overlain by a thin sedimentary cover. Fault structures are poorly developed, and intracrustal reflection patterns are simple and homogeneous, indicating an overall highly stable tectonic setting [18].

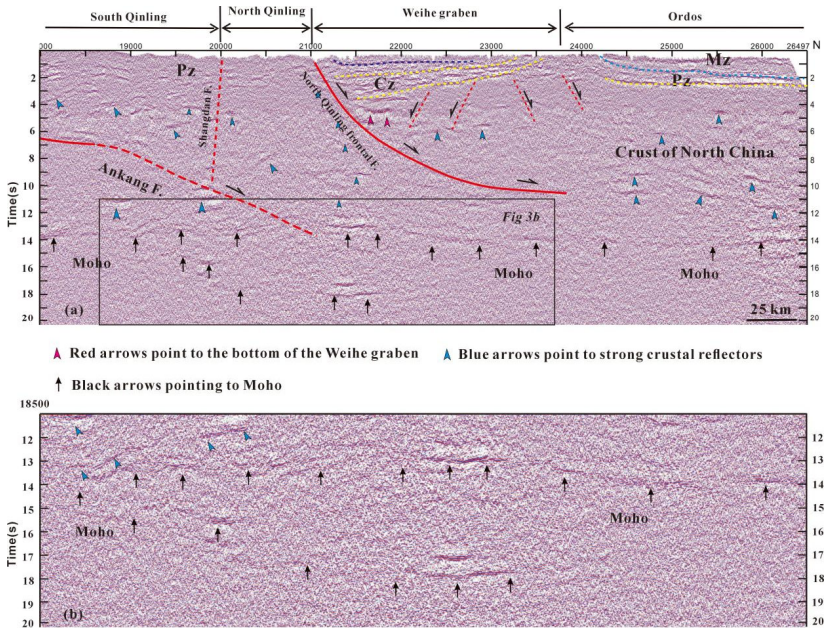



**Figure 3.** (**a**) Depth–migrated seismic reflection profile of the Weihe Graben, (**b**) fine Moho structure beneath the Weihe Graben, migrated seismic reflection profile across the Weihe Graben and adjacent areas.

#### 4.1.3. Reflection Characteristics of the Lower Crust

The lower crust beneath the Sichuan Basin–Dabashan region is generally seismically transparent, with only sparse and discontinuous low-amplitude reflections. Strong reflections occur locally within the Dabashan Orogenic Belt, whereas no widespread lenticular or layered reflectors associated with magmatic activity are observed. These seismic reflection characteristics indicate a relatively homogeneous lower-crustal structure. Beneath the Qinling Orogenic Belt, the lower crust is bounded by the shallow and lower reflector interfaces, within which densely layered and lenticular strong reflectors are widely developed. These reflective zones exhibit good lateral continuity and low structural deformation, indicative of intense material reworking within the crust. In the Weihe Graben segment, lower–crustal reflections above the shallow Moho are chaotic and disordered, whereas continuous and laterally persistent high-amplitude reflective layers occur within the interval between the two Moho reflections (Figure 3b). Lithosphere-penetrating major deep faults vertically displace these strong reflective layers and generate distinct vertically oriented anomalous reflection zones, demonstrating significant fault–related reworking of the lower-crustal structure. The lower crust beneath the southern Ordos Block is characterized by a high degree of structural homogeneity and an overall seismically transparent character. No reflections related to magmatic intrusion are identified, and no evidence of large-scale tectonic reworking is observed, pointing to a stable crustal architecture.

### *4.2. Lithospheric Velocity and Resistivity Characteristics*

#### 4.2.1. Lithospheric Shear-Wave Velocity ($V_S$) Features

Two shear-wave velocity tomographic profiles (Profile A and Profile B) parallel to the deep seismic reflection profile were deployed in this study. The profiles shown in Figure 4 extend northward across the Qinling Orogenic Belt, the Weihe Graben and the Ordos Basin. The topographic map in the lower-right corner illustrates the survey lines, and surface elevation variations for each profile are labelled along the top margin. The Ordos exhibits prominent high-velocity anomalies in the upper mantle, consistent with its nature as an ancient stable craton. In contrast, the Qinling Orogenic Belt shows complex lateral variations: relatively high velocities within the crust and low velocities in the shallow upper mantle. Moho depths vary from approximately 40–50 km and are shallower beneath the extensional basin. These patterns record the structural contrasts between rigid blocks and mobile orogenic belts, which reflect the long-term tectonic evolution of this region.

Moho undulations reveal that the Ordos Basin possesses thicker crust, which progressively thins toward the North Qinling. Significant Moho uplift and pronounced crustal thinning occur beneath the Weihe Graben and the North Qinling Orogenic Belt. Both tomographic profiles show an extensive yellow–coded low-velocity anomaly at depths of 100–200 km below the Moho of the Weihe Graben, indicating a substantial reduction in shear–wave velocity within the lithospheric mantle. In sharp contrast, the deep lithosphere of the main Ordos Craton is dominated by blue–coded high-velocity anomalies. The low–velocity body beneath the Weihe Graben in Profile A covers a larger spatial extent and exhibits stronger concentration, whereas the low–velocity anomaly in Profile B shifts eastward. This observation demonstrates strong lateral heterogeneity of lithospheric–mantle architecture across the study area.

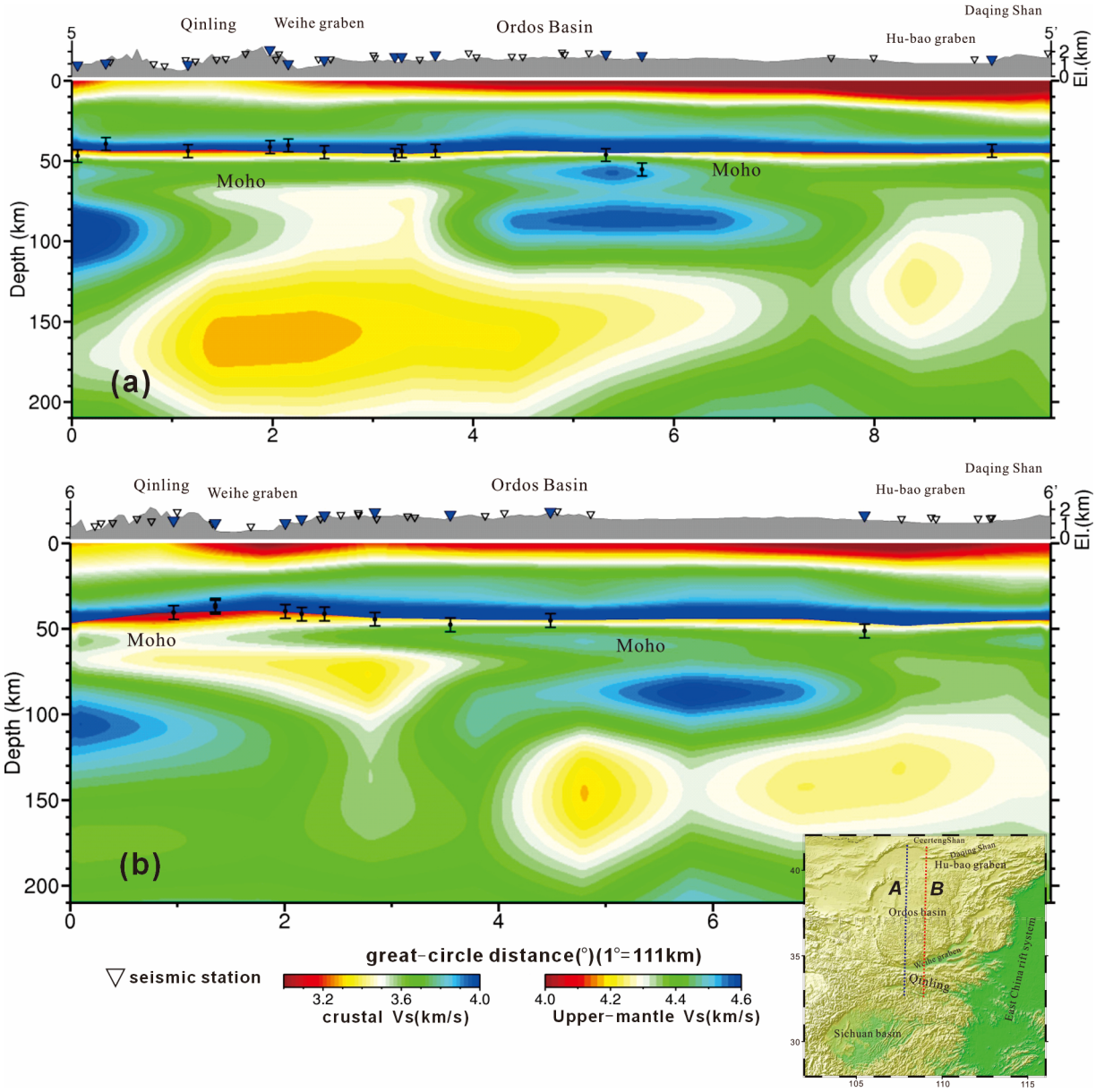



**Figure 4.** (**a**,**b**) S–wave speed transect the Qinling Orogen and the North China (Ordos) [26]. Vertical bars mark the Moho estimated from receiver function analyses beneath seismic stations (inverted triangles) by Feng et al. (2017) [36,38].

#### 4.2.2. Lithospheric Resistivity and P–Wave Velocity ($V_P$) Features

Broadband and long-period magnetotelluric (MT) array surveys were conducted in North China within the SinoProbe project to acquire subsurface resistivity data. The observation network consisted of central and auxiliary sites. Central sites simultaneously recorded broadband MT (Phoenix MTU-5, ≥20 h) and long-period MT (Lemi-417 m, ≥140 h) data, while auxiliary sites only collected broadband MT measurements. A cross electrode layout with GPS time synchronization was adopted. The remote reference technique was applied to suppress strong anthropogenic electromagnetic noise. Spectral analysis and robust impedance estimation were performed on field electromagnetic time series. Apparent resistivity was derived from impedance tensors, with signal frequency controlling the exploration depth. Two−dimensional and three−dimensional inversions were implemented to obtain crustal and mantle resistivity structures [39,40].

Geophysical imaging reveals pronounced spatial contrasts in resistivity and P-wave velocity at crustal (~42/40 km) and upper-mantle (~100 km) depths across the study area. Resistivity models (Figure 5a,b) show that the Ordos Block exhibits high-resistivity anomalies (Log($\rho$) > 2.4 Ω·m) at 42 km depth, whereas low–resistivity anomalies (Log($\rho$) < 1.8 Ω·m) occur beneath the Weihe Graben and the Qinling Orogenic Belt. At 100 km depth, resistivity generally decreases (Log($\rho$) ≈ 1.5–2.0 Ω·m), apart from isolated high-resistivity bodies beneath Zhengzhou and western Ordos. P-wave velocity models (Figure 5c,d) indicate that the Weihe Graben and southern Ordos margin are dominated by low-velocity anomalies (ΔVp < −1.5%) at 40 km depth, while high−velocity bodies (ΔVp > 1.5%) appear in western Qinling and along the eastern Ordos margin. At 100 km depth, a prominent low-velocity core (ΔVp < −3.0%) persists beneath the Weihe Graben and central Ordos, which is surrounded by high-velocity halos (ΔVp > 1.5%) on its southern and eastern sides.

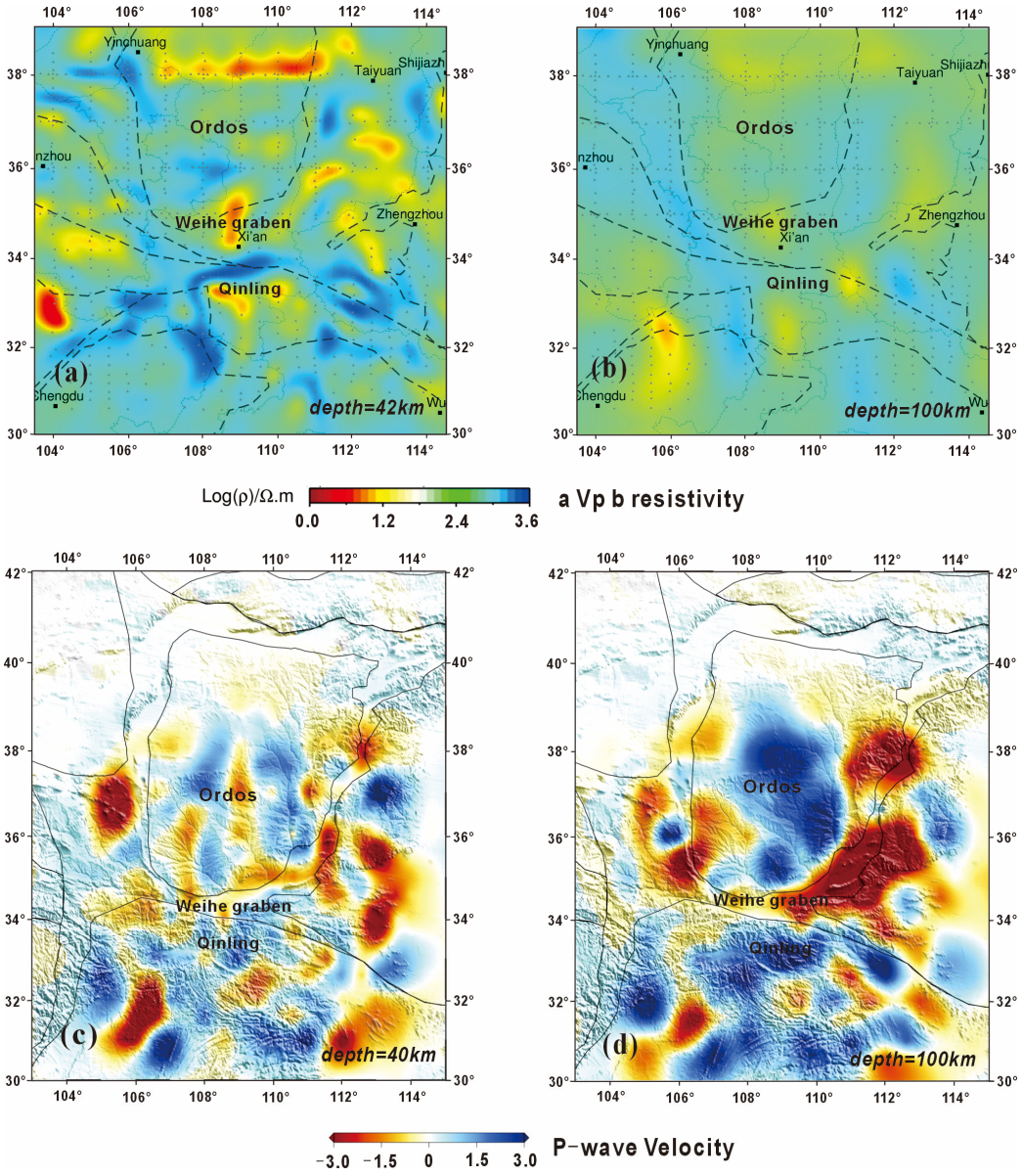



**Figure 5.** (**a**,**b**) Resistivity anomalies at depths of 42 and 100 km, respectively; (**c**,**d**) P−wave velocity perturbations at depths of 40 and 100 km, respectively, beneath the Weihe Graben and surrounding regions [39,40].

Persistent low-resistivity and low-velocity anomalies are imaged from the crust–mantle transition zone down to upper-mantle depths beneath the Weihe Graben. Electrically conductive anomalies (Log($\rho$) $\approx$ 1.2–1.8 $\Omega$·m) are distributed along the graben axis at 42 km, showing good spatial coupling with P-wave velocity deficits ($\Delta$Vp < $-$1.5%) at 40 km. These anomalies extend upward into the mantle (100 km depth), marked by sustained low resistivity (Log($\rho$) $\approx$ 1.5–2.0 $\Omega$·m) and intense low$-$velocity signatures ($\Delta$Vp < $-$3.0%). The spatial overlap of these features suggests elevated temperatures or partial melting within the lithosphere beneath the extensional basin, in sharp contrast to surrounding rigid blocks such as the Ordos Block.

## 5. Discussion

### *5.1. Origin of Moho Doublet*

In this study, reflection seismic was utilized to characterize the fine Moho architecture across a profile spanning from the Sichuan Basin to the southern Ordos Block (Table 2). The results identify a distinct Moho doublet associated with the prominent crustal thinning beneath the North Qinling Orogenic Belt and the Weihe Graben (Figures 2–4). Within the Weihe Graben, the Moho is characterized by a pronounced doublet structure with a substantial vertical separation between the two reflective interfaces. This deep anomalous body that exhibits a lenticular shape with limited lateral extent and tapered terminations indicates that it does not represent a conventional continuous crust–mantle transition zone but corresponds to a residual deep tectonic unit with independent physical properties.

A Moho doublet interface is a typical geophysical manifestation of crust–mantle boundary reworking during continental lithospheric evolution, and its genesis is generally linked to multi-stage tectonic processes including continental collision, crustal thickening, lower-crust high-pressure metamorphism, lithospheric delamination, and post-orogenic extensional overprinting [41–43]. Three end-member models are widely invoked to explain continental Moho doublet occurrences: (1) underplating of mantle-derived mafic magmas [42,44]; (2) crustal stacking and duplicated thickening induced by plate collision [45]; and (3) residual preservation of high-density metamorphosed lower crust after partial delamination [46].

The lower reflector of the Moho doublet can be explained by sills [47]. However, the localized, lens-shaped geometry of the anomaly is difficult to reconcile with extensive magmatic underplating, and geological or geophysical evidence for sufficiently voluminous mafic magmatism is lacking. Evidence supporting the occurrence of voluminous mafic magmatic intrusion capable of producing a continuous, ~15 km thick lenticular anomalous layer is absent, although the region underwent Cenozoic extensional tectonism and associated thermal reorganization of the deep lithosphere. Typical underplated mafic layers are commonly coupled with prominent thermal perturbations and exhibit high-velocity characteristics that grade smoothly into the ambient Moho [48]. In contrast, the deep anomaly recognized in this study possesses a discrete lower boundary and is localized within the present crust–mantle transition interval, inconsistent with pure magmatic underplating. Consequently, mantle underplating may have modified regional lithospheric thermal conditions but is not the primary control on Moho doublet formation beneath the Weihe Graben. Therefore, the mantle underplating model is inadequate to explain the observed Moho doublet feature beneath the Weihe Graben.

Likewise, the collision-driven crustal stacking model cannot fully reproduce the observed structural features. The amalgamation between the North China and South China Plates indeed induced intense crustal shortening and thickening throughout the Qinling Orogen [29]. Nevertheless, pure tectonic stacking generally generates diffuse velocity gra-

dients and broad crust–mantle transition zones [49], rather than the well-defined lenticular deep body with two discrete bounding interfaces imaged in this study.

In comparison, a model involving collision-related lower-crustal metamorphism followed by partial delamination of the orogenic root provides a plausible explanation for the observed Moho doublet. During the Mesozoic collision between the North China and South China Plates, mafic lower-crustal rocks underwent deep burial and high-pressure metamorphism, including eclogitization, which substantially increased their density and rendered parts of the lower crust gravitationally unstable [50]. Dong et al. [23] provided important seismic constraints from the Daba Shan thrust belt for such a density-controlled geodynamic process. Their results suggest that widespread eclogitization affected the mafic lower crust of the northern South China Block following Paleo-Tethys closure. They further suggested that the resulting high-density eclogitized crust could generate substantial negative buoyancy and contribute to prolonged continental convergence [23]. These observations support the inference that high-pressure metamorphism of mafic lower crust can significantly increase crustal density and promote gravitational instability. Although the geometry of a Moho doublet alone cannot uniquely constrain its origin because similar seismic signatures may develop under different tectonic settings [12], the regional tectonic evolution provides an important framework for evaluating its possible formation mechanisms. Subsequent Cenozoic extension and lithospheric destabilization may have triggered gravitational collapse and downward displacement of the dense lower crust [51]. Owing to the complex rheological stratification of the continental lithosphere, delamination may have proceeded incompletely, leaving discrete lower-crustal remnants within the deep lithosphere [52]. During subsequent sinking, these metamorphosed remnants would have been progressively decelerated by viscous resistance from the surrounding lithosphere and upper mantle and ultimately stabilized within the modern crust–mantle transition zone after reaching buoyancy equilibrium [46,53,54]. This multi-stage tectonic evolution provides a plausible mechanism for the development of the Moho doublet beneath the Weihe Graben.

### *5.2. Tectonic Evolution of the Weihe Graben*

Our data clearly reveal prominent Moho uplift beneath the Weihe Graben, accompanied by broadly low shear-wave velocity, low P-wave velocity, and low resistivity anomalies in the deep subsurface, indicative of asthenospheric upwelling. These observations suggest that the formation of the Weihe Graben was closely associated with lithospheric delamination and crustal thinning. Tectonically, the evolutionary characteristics of the Weihe Graben are comparable to those of typical passive rift systems, such as the Rhine Graben and the North Sea Graben [55–59]. Its extensional genesis can be interpreted as follows: far-field extensional stresses associated with remote plate convergence and collision triggered regional extension, which initially induced crustal stretching and thinning and subsequently facilitated asthenospheric uplift [60]. Integrating our seismological observations with previously published geophysical datasets, we constrain the Mesozoic–Cenozoic tectonic evolution of the Weihe Graben (Figure 6).

The Paleo-Tethys Ocean was completely closed by the Late Triassic (ca. 210 Ma), and thrusting in the Dabashan Orogen persisted until the Late Jurassic (ca. 170 Ma) [23,30] (Figure 6a). During the Middle–Late Jurassic, renewed convergence between the South China Plate and the North China Craton triggered intense intracontinental shortening across the Qinling Orogen. This tectonic event caused substantial crustal thickening and established the regional compressional tectonic framework [26] (Figure 6b). Pre-existing major faults, including the Ankang Fault, Shangdan Fault, and northern Qinling Boundary Fault, were established or reactivated and subsequently served as major zones of structural

weakness, laying a fundamental structural foundation for the subsequent development of the Weihe Graben [9]. The study area then experienced a relatively prolonged period of tectonic quiescence lasting approximately 80 Myr.

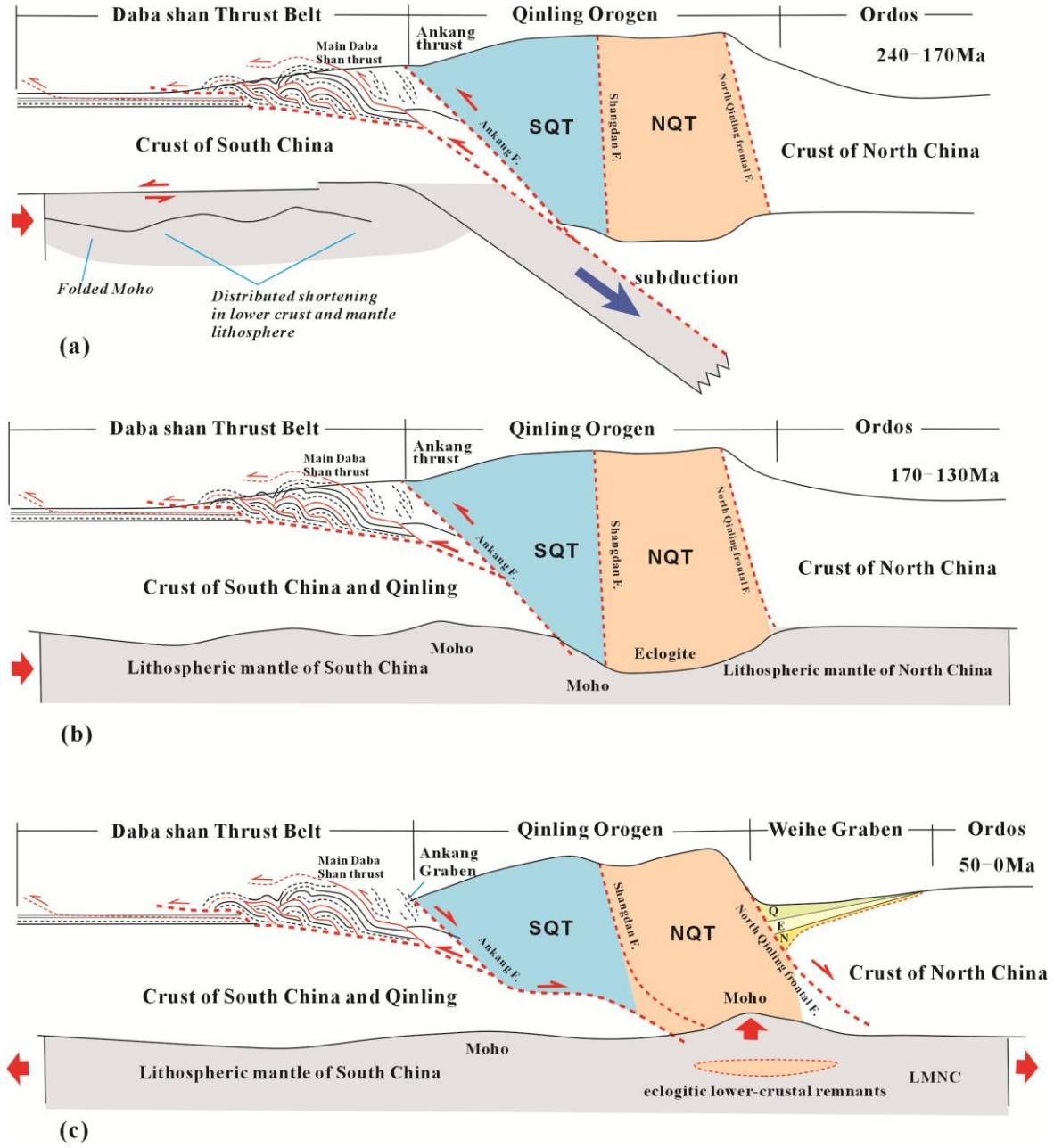



**Figure 6.** (**a**–**c**) Tectonic evolution diagram of the Weihe Graben and adjacent tectonic belts.

Since the Cenozoic, the regional tectonic regime transitioned from compression to extension, with a fundamental reorganization of the regional stress field occurring during the Eocene [61]. The early-stage extensional system was dominated by the rollback of the Pacific Plate, which contributed to the development of a back-arc extensional setting. In the later evolutionary stage, regional tectonics were jointly controlled by the far-field dynamic effects of both Pacific Plate retreat and the India-Eurasia collision [62,63]. Counter-clockwise rotation of the Ordos Block [21] may have induced lithospheric tearing along its southeastern margin and promoted the reactivation of pre-existing faults, including the northern Qinling Boundary Fault and Ankang Fault. This process may have promoted lower-crustal delamination and crustal thinning, thereby creating favorable conditions for

mantle upwelling. The Qinling Orogen underwent differential tilting along major faults, characterized by northward uplift and southward subsidence. Continuous extensional detachment along the northern Qinling margin drove persistent subsidence of the Weihe region, forming the unique asymmetric half-graben morphology of the Weihe Graben, with a deeper southern segment and a shallower northern segment (Figure 6c).

## 6. Conclusions

Based on seismic reflection imaging and deep geophysical constraints, this study characterizes the fine-scale crust–mantle architecture of the Weihe Graben and the North Qinling Orogenic Belt and investigates the deep geodynamic processes responsible for the regional double-Moho structure and the development of the Weihe Graben. The major conclusions are as follows:

(1) The study area exhibits pronounced lateral heterogeneity in crust–mantle architecture across the Qinling Orogenic Belt. A distinctive lenticular double-Moho structure is identified beneath the North Qinling Orogenic Belt and the Weihe Graben, occurring at depths of approximately 36–51 km with a maximum vertical separation of ~15 km. The intervening anomalous layer extends across the lower crust–uppermost mantle transition zone but has a limited lateral extent, indicating strong modification and structural complexity of the crust–mantle boundary.

(2) The Moho doublet beneath the Weihe Graben is unlikely to be explained solely by mantle magmatic underplating or simple crustal stacking. Instead, it primarily reflects high-pressure metamorphism of the lower crust during plate collision and the preservation of residual structures following post-orogenic partial lithospheric delamination. Residues of partially delaminated and metamorphosed lower crust were preserved within the crust–mantle transition zone, thereby producing a persistent double-Moho architecture. Magmatic underplating may have modified the regional thermal structure but was not the dominant mechanism responsible for the formation of the double-Moho structure.

(3) The Weihe Graben represents a composite extensional basin developed under far-field plate-tectonic forcing and evolved through the establishment of a Mesozoic compressional framework followed by Cenozoic extensional reworking. Mesozoic plate collision established the regional compressional system and generated structurally weak fault zones. Subsequent Cenozoic stress reorganization promoted widespread fault reactivation, lower-crustal delamination, and crustal thinning. The combined effects of asthenospheric upwelling and differential block motion contributed to the development of the graben. Counter-clockwise rotation of the Ordos Block and differential reactivation of pre-existing faults promoted sustained extension and subsidence along the northern Qinling margin, producing an asymmetric half-graben geometry characterized by a deeper southern segment and a shallower northern segment.

**Author Contributions:** Conceptualization, L.C., S.D. and Y.P.; methodology, Y.P.; software, L.C.; validation, L.C., S.D. and Y.P.; formal analysis, L.C.; resources, S.D.; data curation, S.D.; writing—original draft preparation, L.C.; writing—review and editing, Y.P., W.S. and S.D.; visualization, L.C.; supervision, S.D., W.S. and Y.P.; funding acquisition, S.D. and W.S. All authors have read and agreed to the published version of the manuscript.

**Funding:** This work was funded by the Deep Earth Probe and Mineral Resources Exploration–National Science and Technology Major Project (No. 2024ZD1001102).

**Institutional Review Board Statement:** Not applicable.

**Informed Consent Statement:** Not applicable.

**Data Availability Statement:** Data is contained within the article.

**Acknowledgments:** The authors are grateful to Chris Juhlin for his valuable comments and constructive suggestions, which have greatly improved the quality of this manuscript.We also appreciate the three anonymous reviewers for their insightful and constructive comments that helped improve this work.

**Conflicts of Interest:** The authors declare no conflicts of interest.

## References

1. Ratschbacher, L.; Hacker, B.R.; Calvert, A.; Webb, L.E.; Grimmer, J.C.; McWilliams, M.O.; Ireland, T.; Dong, S.; Hu, J. Tectonics of the Qinling (Central China): Tectonostratigraphy, geochronology, and deformation history. *Tectonophysics* **2003**, *366*, 1–53. [CrossRef]
2. Dong, Y.; Zhang, G.; Neubauer, F.; Liu, X.; Genser, J.; Hauzenberger, C. Tectonic evolution of the Qinling orogen, China: Review and synthesis. *J. Asian Earth Sci.* **2011**, *41*, 213–237. [CrossRef]
3. Jiang, L.; Li, W.; Dong, Y.; Zhang, L.; Sheir, F.; Feng, Z.; Liang, L.; Wang, C. Cenozoic deformation of the Weihe Graben in central China: Insights from Analogue modeling. *J. Asian Earth Sci.* **2024**, *271*, 106236. [CrossRef]
4. Zhang, H.; Chen, Z.; Lyu, F.; Cai, D.; Lyu, H.; Wang, X.; Cheng, F.; Zhou, Y.; Lu, H. Evolution of the North Qinling Mountains since the Eocene: Evidence from provenance analysis of Cenozoic sediments of the Weihe Basin, central China. *Geol. Soc. Am. Bull.* **2025**, *137*, 3721–3736. [CrossRef]
5. Sun, Y.; Wang, T.; Yin, Q.; Clemens, S.C.; Liu, X.; Ai, L.; Wu, Z.; Qiang, X.; Wang, X.; Chang, H.; et al. Suborbital- and millennial-scale monsoon variability during Pleistocene interglacials. *Proc. Natl. Acad. Sci. USA* **2025**, *122*, e2426353122. [CrossRef] [PubMed]
6. Meng, Q.-R.; Zhang, G.-W. Geologic framework and tectonic evolution of the Qinling orogen, central China. *Tectonophysics* **2000**, *323*, 183–196. [CrossRef]
7. Ai, S.; Zheng, Y.; Riaz, M.S.; Song, M.; Zeng, S.; Xie, Z. Seismic Evidence on Different Rifting Mechanisms in Southern and Northern Segments of the Fenhe-Weihe Rift Zone. *J. Geophys. Res. Solid Earth* **2019**, *124*, 609–630. [CrossRef]
8. Peng, J.B. Tectonic Evolution and Seismic Activity of the Weihe Fault Zone. *Seismol. Geol.* **1992**, *14*, 113–120, (In Chinese with an English Abstract).
9. Peng, J.; Wang, F.; Cheng, Y.; Lu, Q. Characteristics and mechanism of Sanyuan ground fissures in the Weihe Basin, China. *Eng. Geol.* **2018**, *247*, 48–57. [CrossRef]
10. Xu, S.; Mi, N.; Xu, M.; Wang, L.; Li, H.; Yu, D. Crustal structures of the Weihe graben and its surroundings from receiver functions. *Sci. China Earth Sci.* **2013**, *57*, 372–378. [CrossRef]
11. Wang, P.; Huang, Z.; Mi, N.; Xu, M.; Wang, L.; Li, H.; Yu, D.; Huang, H.; Mao, X. Crustal structure beneath the Weihe Graben in central China: Evidence for the tectonic regime transformation in the Cenozoic. *J. Asian Earth Sci.* **2014**, *81*, 105–114. [CrossRef]
12. Tang, Y.; Zhou, S.; Chen, Y.J.; Sandvol, E.; Liang, X.; Feng, Y.; Jin, G.; Jiang, M.; Liu, M. Crustal structures across the western Weihe Graben, North China: Implications for extrusion tectonics at the northeast margin of Tibetan Plateau. *J. Geophys. Res. Solid Earth* **2015**, *120*, 5070–5081. [CrossRef]
13. Tapponnier, P.; Peltzer, G.; Le Dain, A.Y.; Armijo, R.; Cobbold, P.R. Propagating extrusion tectonics in Asia: New insights from simple experiments with plasticine. *Geology* **1982**, *10*, 611–616. [CrossRef]
14. Yin, A. Cenozoic tectonic evolution of Asia: A preliminary synthesis. *Tectonophysics* **2010**, *488*, 293–325. [CrossRef]
15. Zhang, Y.Q.; Shi, W.; Dong, S.W. Neotectonics of North China: Interplay between Far-Field Effect of India-Eurasia Collision and Pacific Subduction-Related Deep-Seated Mantle Upwelling. *Acta Geol. Sin.* **2019**, *93*, 971–1001, (In Chinese with an English Abstract).
16. Li, M.; Wei, Y.; Wu, T.; Li, J. Crustal isostatic state and lower crust delamination beneath the Qinling Orogenic Belt: Constraints from receiver function imaging. *Gondwana Res.* **2022**, *103*, 54–63. [CrossRef]
17. Li, H.; Gao, R.; Huang, X.; Wang, H.; Guo, X.; Liang, H.; Tan, X.; Liu, X.; Yang, Z. Triassic convergence and tectonic evolution of the West Qinling orogen: Constraints from reflection-seismology imaging. *Gondwana Res.* **2023**, *122*, 1–10. [CrossRef]
18. Ren, J.; Peng, J.B.; Wang, F.Y.; Liu, C.; Feng, X.J.; Dai, W.Q. Characteristics of Deep Crustal Structure beneath the Weihe Basin and Its Adjacent Areas. *Chin. J. Geophys.* **2012**, *55*, 2939–2947, (In Chinese with an English Abstract). [CrossRef]
19. Ren, J.; Feng, X.J.; Wang, F.Y.; Peng, J.B.; Liu, C.; Dai, W.Q.; Li, G.Y.; Zhang, Y.; Ma, J. Fine Crustal Structure of the Xi'an Depression in the Weihe Basin Revealed by Deep Seismic Reflection Profile. *Chin. J. Geophys.* **2013**, *56*, 513–521, (In Chinese with an English Abstract). [CrossRef]
20. Li, H.; Gao, R.; Xiong, X.; Wang, H.; Li, W. Moho fabrics of North Qinling Belt, Weihe Graben and Ordos Block in China constrained from large dynamite shots. *Geophys. J. Int.* **2017**, *209*, 643–653. [CrossRef]

21. Zhang, Y.; Liao, C.; Shi, W.; Zhang, T.; Guo, F. Jurassic Deformation in and Around the Ordos Basin, North China. *Earth Sci. Front.* **2007**, *14*, 182–196. [CrossRef]
22. Liu, C.; Ji, L.; Zhu, L.; Xu, C.; Zhang, W.; Qiu, J.; Xiong, G. Present-Day Three-Dimensional Deformation across the Ordos Block, China, Derived from InSAR, GPS, and Leveling Observations. *Remote Sens.* **2023**, *15*, 2890. [CrossRef]
23. Dong, S.; Gao, R.; Yin, A.; Guo, T.; Zhang, Y.; Hu, J.; Li, J.; Shi, W.; Li, Q. What drove continued continent-continent convergence after ocean closure? Insights from high-resolution seismic-reflection profiling across the Daba Shan in central China. *Geology* **2013**, *41*, 671–674. [CrossRef]
24. Li, J.; Dong, S.; Yin, A.; Zhang, Y.; Shi, W. Mesozoic tectonic evolution of the Daba Shan Thrust Belt in the southern Qinling orogen, central China: Constraints from surface geology and reflection seismology. *Tectonics* **2015**, *34*, 1545–1575. [CrossRef]
25. Cook, F.A. Fine structure of the continental reflection Moho. *Geol. Soc. Am. Bull.* **2002**, *114*, 64–79. [CrossRef]
26. Zhang, Y.; Dong, S.; Wang, H.; Feng, M.; Thybo, H.; Li, J.; Gao, R.; Shi, W. Coupled Lithospheric Deformation in the Qinling Orogen, Central China: Insights from Seismic Reflection and Surface-Wave Tomography. *Geophys. Res. Lett.* **2022**, *49*, e2022GL097760. [CrossRef]
27. Dong, Y.; Safonova, I.; Wang, T. Tectonic evolution of the Qinling orogen and adjacent orogenic belts. *Gondwana Res.* **2016**, *30*, 1–5. [CrossRef]
28. Ji, C.; Han, C.; Wang, X.; Bokelmann, G.; Huang, Z. Differential Craton Destruction Controlled by Fossil Structures in the Central North China Craton. *Geophys. Res. Lett.* **2026**, *53*, e2025GL119472. [CrossRef]
29. Zhang, G.; Meng, Q.; Lai, S. Tectonics and structure of Qinling orogenic belt. *Sci. China Ser. B* **1995**, *38*, 1379–1394.
30. Zhang, Y.; Dong, S.; Li, J. Late Paleogene sinistral strike-slip system along east Qinling and in southern North China: Implications for interaction between collision-related block trans-rotation and subduction-related back-arc extension in East China. *Tectonophysics* **2019**, *769*, 228181. [CrossRef]
31. Li, Y.; Xiong, X.; Feng, Y. Mesozoic uplift of the Dabashan and Micangshan-Hannan Dome in the South Qinling orogenic belt. *Sci. China Earth Sci.* **2022**, *65*, 426–436. [CrossRef]
32. Qi, K.; Ren, Z.L.; Zhang, M.T.; Ma, Q.; Yang, Y.; Liu, R.C. Detrital Zircon Geochronology, Geochemistry and Tecto-Sedimentary Significance of the Late Paleozoic-Mesozoic in the Weihe Area and Its Adjacent Regions. *Acta Petrol. Sin.* **2020**, *36*, 1897–1912, (In Chinese with an English Abstract). [CrossRef]
33. Zhang, Y.Q.; Mercier, J.L.; Vergély, P. Extension in the graben systems around the Ordos (China), and its contribution to the extrusion tectonics of south China block: Inference from Quaternary fault kinematics. *Tectonophysics* **1998**, *285*, 27–52. [CrossRef]
34. Yang, P.; Ren, Z.L.; Zhang, J.G.; Cui, J.P. Discussion on the Coupling Relationship of Sedimentary-Tectonic Migration in the Cenozoic Weihe Basin with the Weibei Uplift and Eastern Qinling. *Chin. J. Geol.* **2018**, *53*, 1320–1338, (In Chinese with an English Abstract). [CrossRef]
35. Lyu, H.; Lu, H.; Wang, Y.; Zhang, H.; Wang, Y.; Wang, K.; Lai, W.; Liu, Z.; Li, Y.; Ji, J. East Asian paleoclimate change in the Weihe Basin (central China) since the middle Eocene revealed by clay mineral analysis. *Sci. China Earth Sci.* **2021**, *64*, 1285–1304. [CrossRef]
36. Feng, M.; An, M.; Dong, S. Tectonic history of the Ordos Block and Qinling Orogen inferred from crustal thickness. *Geophys. J. Int.* **2017**, *210*, 303–320. [CrossRef]
37. Gan, J.S.; Liu, S.W.; Li, Y.J. Tectonic Development Characteristics of the Yuehe Pull-apart Basin in Ankang, South Qinling. *J. Geod. Geodyn.* **2002**, *22*, 101–105, (In Chinese with an English Abstract). [CrossRef]
38. Feng, M.; An, M. Lithospheric structure of the Chinese mainland determined from joint inversion of regional and teleseismic Rayleigh-wave group velocities. *J. Geophys. Res. Solid Earth* **2010**, *115*, 1–16. [CrossRef]
39. Ouro-Djobo, S.B.; Wei, W.B.; Ye, G.F.; Jin, S.; Jing, J.E.; Ji, L.Z.; Dong, H.; Zhang, L.T.; Yin, Y.T.; Xie, C.L. Experiments of magnetotelluric observation network on North China and lithospheric conductivity structure from fast imaging method. *Chin. J. Geophys.* **2018**, *61*, 2508–2524, (In Chinese with an English abstract). [CrossRef]
40. Ji, L.Z.; Ye, G.F.; Jin, S.; Ma, X.Z.; Wei, W.B.; Wang, S.; Qi, J.L.; Lei, Q.; Gu, J.F. Spatial heterogeneity of the lithospheric destruction of the North China Craton: Evidence from an extended magnetotelluric sounding profile. *Front. Earth Sci.* **2023**, *10*, 1105274. [CrossRef]
41. Thybo, H.; Nielsen, C.A. Magma-compensated crustal thinning in continental rift zones. *Nature* **2009**, *457*, 873–876. [CrossRef] [PubMed]
42. Yuan, X.; Balázs, A.; Gerya, T.; Xiong, X. Uplift of the Tibetan Plateau driven by mantle delamination from the overriding plate. *Nat. Geosci.* **2024**, *17*, 721–727. [CrossRef] [PubMed]
43. Jagoutz, O.; Behn, M.D. Foundering of lower island-arc crust as an explanation for the origin of the continental Moho. *Nature* **2013**, *504*, 131–134. [CrossRef] [PubMed]
44. Artemieva, I.M.; Thybo, H. EUNAseis: A seismic model for Moho and crustal structure in Europe, Greenland, and the North Atlantic region. *Tectonophysics* **2013**, *609*, 97–153. [CrossRef]

45. Zhou, Z.; Thybo, H.; Artemieva, I.M.; Kusky, T.; Tang, C.C. Crustal melting and continent uplift by mafic underplating at convergent boundaries. *Nat. Commun.* **2024**, *15*, 9039. [CrossRef] [PubMed]
46. Krystopowicz, N.J.; Currie, C.A. Crustal eclogitization and lithosphere delamination in orogens. *Earth Planet. Sci. Lett.* **2013**, *361*, 195–207. [CrossRef]
47. Singh, S.C.; Harding, A.J.; Kent, G.M.; Sinha, M.C.; Combier, V.; Bazin, S.; Tong, C.H.; Pye, J.W.; Barton, P.J.; Hobbs, R.W.; et al. Seismic reflection images of the Moho underlying melt sills at the East Pacific Rise. *Nature* **2006**, *442*, 287–290. [CrossRef] [PubMed]
48. Thybo, H.; Artemieva, I.M. Moho and magmatic underplating in continental lithosphere. *Tectonophysics* **2013**, *609*, 605–619. [CrossRef]
49. Carbonell, R.; Levander, A.; Kind, R. The Mohorovičić discontinuity beneath the continental crust: An overview of seismic constraints. *Tectonophysics* **2013**, *609*, 353–376. [CrossRef]
50. Huang, F.; Li, S.-G.; Dong, F.; He, Y.-S.; Chen, F.-K. High-Mg adakitic rocks in the Dabie orogen, central China: Implications for foundering mechanism of lower continental crust. *Chem. Geol.* **2008**, *255*, 1–13. [CrossRef]
51. Molnar, P.; Houseman, G.A. Effects of a low-viscosity lower crust on topography and gravity at convergent mountain belts during gravitational instability of mantle lithosphere. *J. Geophys. Res. Solid Earth* **2015**, *120*, 537–551. [CrossRef]
52. Li, Z.H.; Liu, M.; Gerya, T. Lithosphere delamination in continental collisional orogens: A systematic numerical study. *J. Geophys. Res. Solid Earth* **2016**, *121*, 5186–5211. [CrossRef]
53. Gao, S.; Rudnick, R.L.; Yuan, H.-L.; Liu, X.-M.; Liu, Y.-S. Recycling lower continental crust in the North China craton. *Nature* **2004**, *432*, 892–897. [CrossRef] [PubMed]
54. Peng, L.; Liu, L.; Liu, L. The fate of delaminated cratonic lithosphere. *Earth Planet. Sci. Lett.* **2022**, *594*, 117740. [CrossRef]
55. Brune, S.; Kolawole, F.; Olive, J.-A.; Stamps, D.S.; Buck, W.R.; Buiter, S.J.H.; Furman, T.; Shillington, D.J. Geodynamics of continental rift initiation and evolution. *Nat. Rev. Earth Environ.* **2023**, *4*, 235–253. [CrossRef]
56. Phillips, T.B.; Fazlikhani, H.; Gawthorpe, R.L.; Fossen, H.; Jackson, C.A.-L.; Bell, R.E.; Faleide, J.I.; Rotevatn, A. The Influence of Structural Inheritance and Multiphase Extension on Rift Development, the NorthernNorth Sea. *Tectonics* **2019**, *38*, 4099–4126. [CrossRef]
57. Fazlikhani, H.; Fossen, H.; Gawthorpe, R.L.; Faleide, J.I.; Bell, R.E. Basement structure and its influence on the structural configuration of the northern North Sea rift. *Tectonics* **2017**, *36*, 1151–1177. [CrossRef]
58. Manatschal, G.; Lavier, L.; Chenin, P. The role of inheritance in structuring hyperextended rift systems: Some considerations based on observations and numerical modeling. *Gondwana Res.* **2015**, *27*, 140–164. [CrossRef]
59. Anikiev, D.; Cacace, M.; Bott, J.; Gomez Dacal, M.L.; Scheck-Wenderoth, M. Influence of Lithosphere Rheology on Seismicity in an Intracontinental Rift: The Case of the Rhine Graben. *Front. Earth Sci.* **2020**, *8*, 592561. [CrossRef]
60. Ziegler, P.A.; Cloetingh, S. Dynamic processes controlling evolution of rifted basins. *Earth-Sci. Rev.* **2004**, *64*, 1–50. [CrossRef]
61. Lu, J.; Rao, S.; Hu, S.; Huang, S.; Zhang, Q.; Li, W.; Yang, Y. Cenozoic tectono-thermal evolution of the Weihe Basin, Central China. *Int. Geol. Rev.* **2024**, *66*, 3225–3241. [CrossRef]
62. Shi, W.; Chen, L.; Chen, X.; Cen, M.; Zhang, Y. The Cenozoic tectonic evolution of the faulted basins in the northern margin of the Eastern Qinling Mountains, Central China: Constraints from fault kinematic analysis. *J. Asian Earth Sci.* **2019**, *173*, 204–224. [CrossRef]
63. Chen, X.; Dong, S.; Shi, W.; Zuza, A.V.; Li, Z.; Chen, P.; Liu, J.; Hu, J.; Han, B. Magnetostratigraphic ages of the Cenozoic Weihe and Shanxi Grabens in North China and their tectonic implications. *Tectonophysics* **2021**, *813*, 228914. [CrossRef]


**Disclaimer/Publisher's Note:** The statements, opinions and data contained in all publications are solely those of the individual author(s) and contributor(s) and not of MDPI and/or the editor(s). MDPI and/or the editor(s) disclaim responsibility for any injury to people or property resulting from any ideas, methods, instructions or products referred to in the content.